The Conformational Manifold of Ferricytochrome *c* Explored by Visible and Far-UV Electronic Circular Dichroism Spectroscopy[†]

Andrew Hagarman,[‡] Laura Duitch,[‡,§] and Reinhard Schweitzer-Stenner*[,‡]

Department of Chemistry and Department of Bioscience and Biotechnology, Drexel University, Philadelphia, Pennsylvania 19104

Received April 24, 2008; Revised Manuscript Received June 16, 2008

ABSTRACT: The oxidized state of cytochrome *c* is a subject of continuous interest, owing to the multitude of conformations which the protein can adopt in solution and on surfaces of artificial and cell membranes. The structural diversity corresponds to a variety of functions in electron transfer, peroxidase and apoptosis processes. In spite of numerous studies, a comprehensive analysis and comparison of native and non-native states of ferricytochrome *c* has thus far not been achieved. This results in part from the fact that the influence of solvent conditions (i.e., ionic strength, anion concentration, temperature dependence of pH values) on structure, function and equilibrium thermodynamics has not yet been thoroughly assessed. The current study is a first step in this direction, in that it provides the necessary experimental data to compare different non-native states adopted at high temperature and alkaline pH. To this end, we employed visible electronic circular dichroism (ECD) and absorption spectroscopy to probe structural changes of the heme environment in bovine and horse heart ferricytochrome *c* as a function of temperature between 278 and 363 K at different neutral and alkaline pH values. A careful selection of buffers enabled us to monitor the partial unfolding of the native state at room temperature while avoiding a change to an alkaline state at high temperatures. We found compelling evidence for the existence of a thermodynamic intermediate of the thermal unfolding/folding process, termed III_h, which is structurally different from the alkaline states, IV_1 and IV_2, contrary to current belief. At neutral or slightly acidic pH, III_h is populated in a temperature region between 320 and 345 K. The unfolded state of the protein becomes populated at higher temperatures. The ECD spectra of the B-bands of bovine and horse heart cytochrome *c* (pH 7.0) exhibit a pronounced couplet that is maintained below 343 K, before protein unfolding replaces it by a rather strong positive Cotton band. A preliminary vibronic analysis of the B-band profile reveals that the couplet reflects a B-band splitting of 350 cm^{-1}, which is mostly of electronic origin, due to the internal electric field in the heme cavity. Our results suggest that the conformational transition from the native state, III, into a thermally activated intermediate state, III_h, does not substantially affect the internal electric field and causes only moderate rearrangements of the heme pocket, which involves changes, rather than a rupture, of the Fe^{3+}−M80 linkage. In the unfolded state, as well as in the alkaline states IV and V, the band splitting is practically eliminated, but the positive Cotton effect observed for the B-band suggests that the proximal environment, encompassing H18 and the two cysteine residues 14 and 17, is most likely still intact and covalently bound to the heme chromophore. Both alkaline states IV and V were found to melt via intermediate states. Unfolded states probed at neutral and alkaline pH can be discriminated, owing to the different intensities of the Cotton bands of the respective B-band transitions. Differences between the ECD intensities of the B-bands of the different unfolded states and alkaline states most likely reflect different degrees of openness of the corresponding heme crevice.

Cytochrome *c* is a comparatively small (MW ∼ 12.4 kDa) heme protein that mediates the electron transfer from cytochrome *c* reductase to cytochrome *c* oxidase (*1*). The protein contains a single heme group, the central iron atom of which is coordinated to a histidine (H18[1]) and a methionine (M80). Over the last forty years cytochrome *c* has served as a model system for studying electron transfer processes and protein folding. Additional interest in this protein has recently been created by the discovery of its role in apoptosis and its conformationally dependent peroxidase activity (*2–4*). The ferri state of cytochrome *c* is pH dependent in that it adopts six total native and non-native states over the pH range 1−15, whereas the ferro state adopts a stable structure over most of this pH range. The relevance of non-native states stems from the facts (a) that they constitute intermediate states of protein unfolding and denaturation processes (*5*) and (b) that non-native states of ferricytochrome *c* are of general relevance for understanding the protein's function,

[†] We acknowledge financial support to R.S.-S. from the NSF Grant MCB 0318749. L.D. received a Maryanoff summer research fellowship for first year undergraduate students. Drexel University, Chemistry Department, funded, in part, the SRCD measurements at Brookhaven National Laboratories.

* Corresponding author. E-mail: rschweitzer-stenner@drexel.edu.
[‡] Department of Chemistry.
[§] Department of Bioscience and Biotechnology.

[1] Abbreviations: ECD, electronic circular dichroism; CT, charge transfer; M80, methionine 80; H18, histidine 18; F82, phenylalanine 82; W59, tryptophan 59.

10.1021/bi800729w CCC: $40.75 © 2008 American Chemical Society
Published on Web 08/15/2008

because they, rather than the so-called native state, seem to resemble conformations adopted in electron transfer processes, peroxidase activity and apoptosis (*6*). The native state, referred to as state III, is adopted at neutral pH. At more acidic pH values (pH 2−4) state II is populated, constituting a partially folded protein structure (*7*). At even lower pH values (pH < 2) an unfolded state, termed state I, is adopted by the protein at low ionic strength, whereas anion binding can switch it back to a molten globule-like state (*8*). A well-documented alkaline transition into states IV_1 and IV_2 occurs around pH 9−11, which has been studied quite extensively for yeast cytochrome *c*. Mauk, Hildebrand and co-workers discovered that state IV comprises two substates with different lysines (K73 and K79) as axial ligands and different effective p*K*-values for the corresponding alkaline transitions (*9, 10*). This alkaline transition is generally thought to create a more open heme crevice. In each substate the respective lysine replaces the axial M80 ligand. Optical spectroscopy investigations of Blouin et al. indicate that the situation is even more complicated for horse heart cytochrome *c*, for which these authors found evidence for the existence of another alkaline conformer which is separated from IV_1 and IV_2 by a rather high energy barrier (*11*).

With respect to complexes of cytochrome *c* with cytochrome *c* oxidase, another state, V, which is adopted at pH values above 11.0, seems to be relevant as well (*12*). In this state the lysine ligand of the heme iron is thought to be replaced by hydroxide, but a final identification of the sixth ligand has not yet been accomplished. The state is generally considered to be mostly molten globule with an intact secondary and a perturbed tertiary structure. Whether a denatured molten globule state adopted at more alkaline pH values is different from V has to be clarified (*13*).

The thermal stability of the oxidized and reduced states of cytochrome *c* is also vastly different. While the thermal unfolding of ferrocytochrome *c* generally requires temperatures above 100 °C (373 K) (*14*), the native state III of ferricytochrome *c* starts the unfolding process at considerably lower temperatures (40 °C (313 K) to 70 °C (343 K). Generally, the unfolding of ferricytochrome *c* involves the population of a thermodynamic intermediate III_h above 50 °C (323 K) and the subsequent unfolding into the state U above 70 °C (343 K) (*15*). The III → III_h transition is generally probed by the 695 nm charge transfer band, which disappears or is considerably weaker in III_h (*16*). Based on the ^1H and ^{13}C NMR spectra of oxidized horse heart cytochrome *c*, Taler et al. argued that M80 is replaced by another amino acid residue in III_h (*5*). The authors concluded that III_h is identical with the aforementioned alkaline state IV populated between pH 9.0 and 11.0 at room temperature (*17*). Both the thermal and the alkaline transition cause a substantial decrease of the redox potential (*18*). Taler et al. rationalized the identity of states III_h and IV as being caused by a drastic decrease of the effective p*K*-value of the alkaline transition, which allows a population of the alkaline state at neutral pH and high temperatures (*5*). The downshift of the apparent p*K*-value has indeed been observed in several thermodynamic and electrochemical experiments (*18, 19*). However, several lines of yet not fully appreciated evidence argue against the identity of III_h and IV. First, Battistuzzi et al. showed that the van't Hoff plot of the apparent p*K*-value of the alkaline transition is biphasic, which these authors interpreted as indicative of the existence of a neutral high temperature state which is identical neither with the alkaline nor with the native state (*19*). Recently, Schweitzer-Stenner et al. showed that the 695 nm absorption and the corresponding circular dichroism band of horse heart ferricytochrome *c* decrease above 50 °C (323 K) at pH 6 and 7 (*20*). The transition temperatures of the respective III → III_h transitions at these pH values are practically identical. If III_h was indeed identical with IV, the transition between them should not be detectable in the temperature range between 0° (273 K) and 60 °C (333 K) at pH 6. In view of these contradictions it is desirable to reinvestigate the identity of state III_h.

While numerous studies have been performed to explore thermodynamics and electrochemistry of the above conformational transitions (*5, 9, 11, 18, 19*), information about the structural properties of the involved non-native states is limited. Where optical and resonance Raman spectra indicate that the low-spin state of the heme iron is maintained in both III_h and IV (*9*), it is unclear to what extent the corresponding conformational transitions change functionally relevant heme−protein interactions and the structure of the heme macrocycle. Concomitant changes of the secondary structure are indicated by far-UV electronic circular dichroism (ECD) spectra and by FTIR data for III → III_h (*21*), but their quantitative assessment and specific assignment to distinct regions of the protein have not yet been achieved.

The current study was guided by the hypothesis that the thermally excited intermediate state, III_h, is thermodynamically and structurally distinct from the frequently investigated alkaline states, IV_1 and IV_2, contrary to the conclusions drawn by Taler et al. (*5*). The examination of this hypothesis was embedded into a general spectroscopic investigation of non-native ferricytochrome *c* conformations adopted at neutral and alkaline pH. To this end we utilized visible and, to a limited extent, far-UV electronic circular dichroism (ECD) spectroscopy. While visible ECD has been frequently used to monitor structural changes of the heme group in a variety of cytochrome *c* derivatives (*21–25*), the structural and physical interpretation of the observed spectra and their respective changes remain speculative, owing to a lack of quantitative analysis. Woody and associates provided a physical picture of the origin of heme circular dichroism, namely, interactions between the electronic transitions of the heme and the protein environment (*26*). In this context, dipolar coupling between the heme group and adjacent aromatic side chains are of particular relevance. A study from this group also showed that nonplanar deformations can substantially modulate the ECD spectrum of the Soret (B) band (*27*). Only recently, Dragomir et al. showed that B- and Q-band CD spectra of both ferri- and ferrocytochrome *c* are diagnostic of band splitting, which arises from electronic and vibronic perturbations of the heme group (*28*). A similar discovery has been made for deoxymyoglobin and MbCN (*29*). These findings prompted us to combine visible ECD and absorption spectroscopy to probe heme−protein interactions in bovine heart cytochrome *c* (bhc) as a function of temperature between 278 and 363 K for different pH values between 7.0 and 11.5. Bovine cytochrome *c* has been selected because compared with horse heart and particularly yeast cytochrome *c* is less prone to aggregation at very high temperatures. However, some experiments were also carried

out with horse heart cytochrome *c* (hhc) for a mutual confirmation of the obtained results and for checking whether small structural differences are caused by the substitutions S(47) → T, G(60) → K and G(89) → T (*30*). The set of spectra obtained in our study allows a comparison of the states III, III_h, IV and V. Moreover, the spectra allow for us to check for the existence of thermally populated intermediate states for states IV and V. Our experimental data enable us to compare heme−protein interactions in the folding/unfolding intermediate III_h, in the alkaline states IV and V and in the thermally unfolded state (U) which the protein adopts above 70 °C (343 K). At neutral pH, concomitant changes of the secondary structure associated with the III → III_h transitions were probed by far UV-ECD measurements. A representative set of the obtained spectra were analyzed in terms of a recently developed vibronic coupling model (*29*). The results of this analysis yielded the electronic perturbations of the excited B-state in the investigated states. We argue that these perturbations result predominantly from a Stark effect, owing to the internal electric field at the heme (*29, 31*).

MATERIAL AND METHODS

Materials. Cytochrome *c* from bovine heart and horse heart was purchased from Sigma-Aldrich (St. Louis, MO) and dissolved (a) in a 0.1 M Tris·HCl (Trizma) buffer (pH 7.2, $I = 0.1$ M), from Sigma-Aldrich (St. Louis, MO) and (b) in a 1 mM MOPS (3-(*N*-morpholino)propanesulfonic acid) buffer (pH 7 and 8.5, $I = 0.001$ M), from Sigma-Aldrich (St. Louis, MO). An alkaline solution was obtained with a 50 mM Bis/Tris buffer (pH 9.6) titrated with small amounts of 0.1 M NaOH solution to achieve pH values of 10.5 and 11.5. Complete oxidation was achieved by adding a small amount of potassium ferricyanide obtained from Fisher Scientific (Pittsburgh, PA) to the sample. Subsequently, the excess oxidant was removed from the sample by dialysis against the respective buffer solution.

CD Measurements. We prepared 50 μM protein solutions for visible ECD and absorption measurements. The B-band spectra were measured as a function of temperature in digital form with a J-810 spectrapolarimeter (Jasco Inc.), in the spectral region from 350 to 550 nm. Far-UV ECD spectra were measured in the spectral region from 185−240 nm with a protein concentration of 0.5 mM in Tris HCl buffer, measured with the same instrument and the following parameters. The temperature was controlled by a Peltier heating/cooling system from 5°−90 °C (±0.1 °C) (278−363 K). Between ten and twenty accumulations were averaged using a 5 nm bandwidth, a 500 nm/min scanning speed, and a 0.1 or 0.5 nm data pitch. Additionally, a background subtraction was carried out for all the spectra using similar parameters. A 1.0 mm quartz cell (Helma) was used for all measurements. The pH was measured before and after each measurement.

Synchrotron radiation circular dichroism (SRCD) measurements were performed at Brookhaven National Laboratories. Beamline U11 was used to measure the SRCD spectra in the spectral region from 170−260 nm of horse and bovine heart cytochrome *c*. The proteins were dissolved in 0.1 M TrisHCl buffer at a concentration of 6 mg/mL (~0.5 mM). Three accumulations were averaged at each indicated temperature, controlled by a Peltier heating/cooling system, with similar parameters used for the background subtraction.

RESULTS

This section of the paper is organized as follows. First, we introduce a protocol which enables us to unambiguously discriminate, thermodynamically, between the states III_h and IV. Second, we detail temperature dependent far-UV ECD spectra to elucidate the secondary structure of III_h. Next, we analyze representative ECD and absorption spectra by means of a recently developed algorithm to estimate the splitting of the B-band, owing to electronic and vibronic perturbations (*29*). Finally, we characterize differences between alkaline states as well as thermally populated intermediate states. In what follows we do not discriminate between the substates IV_1 and IV_2 and V_1 and V_2 discovered by Döpner et al. (*9*).

Thermal Unfolding of the Native State III. To separate the thermal unfolding of the native state from the alkaline III → IV transition, we had to select experimental conditions which allow the protein to sample the native state at ambient temperatures and avoid a detectable population of the alkaline state at high temperatures. To this end, we used a 0.1 M Tris HCl buffer to ensure that the aforementioned requirements were met. The pH value of this buffer decreases by 0.03 pH units per °C increase of temperature. The pH of this buffer was 7.6 at the lowest temperature (278 K). With rising temperature, the pH decreased to reach 6.3 at 333 K and 5.6 at 363 K. This downshift of the pH value is comparable with the temperature dependence of the effective p*K* value of the III → IV transition, for which Battistuzzi et al. obtained 9.4 at 278 K and 7.9 at 340 K for the ionic strength of 0.1 M used in our experiment (*18, 19*). Thus, we kept the "distance" between the actual pH value of our experiment and the p*K* value of the III → IV transition approximately constant, so that a detectable occupation of state IV at high temperatures can be ruled out. Figure 1 exhibits the corresponding ECD and absorption spectra of bhc and hhc in the aforementioned buffer measured as function of temperature between 278 K and 363 K in increments of 5 K. The rather high ionic strength, which ensures the binding of 2 (3) Cl^- ions to the surface of bhc (hhc) (*18*), resembles the conditions frequently used for exploring the temperature dependence of ferricytochrome *c* (*15, 16, 30, 32*). The ECD spectra display a pronounced, slightly negatively biased couplet at room temperature, which gradually changes into a more symmetric couplet with increasing temperature between 278 and 338 K. The insets of Figures 1B and 1D display the respective extinction value, ε_{max}, at the peak position as a function of temperature. ε_{max} decreases with rising temperatures between 278 and 333 K and subsequently increases between 343 and 363 K. This second phase additionally involves a blueshift of the absorption spectrum. At higher temperatures the CD couplet disappears and is replaced by a slightly blueshifted, positive Cotton band. The temperature dependence of the $\Delta\varepsilon$ values at the maximum ($\Delta\varepsilon_{max}$), central ($\Delta\varepsilon_{cent}$) and minimum ($\Delta\varepsilon_{min}$) position of the couplet are displayed in Figure 2. As expected, corresponding values of hhc and bhc are very similar, but hhc systematically exhibits slightly more negative values at the minimum and the central position of the couplet between 278 and 343 K. Interestingly, the three $\Delta\varepsilon$ values

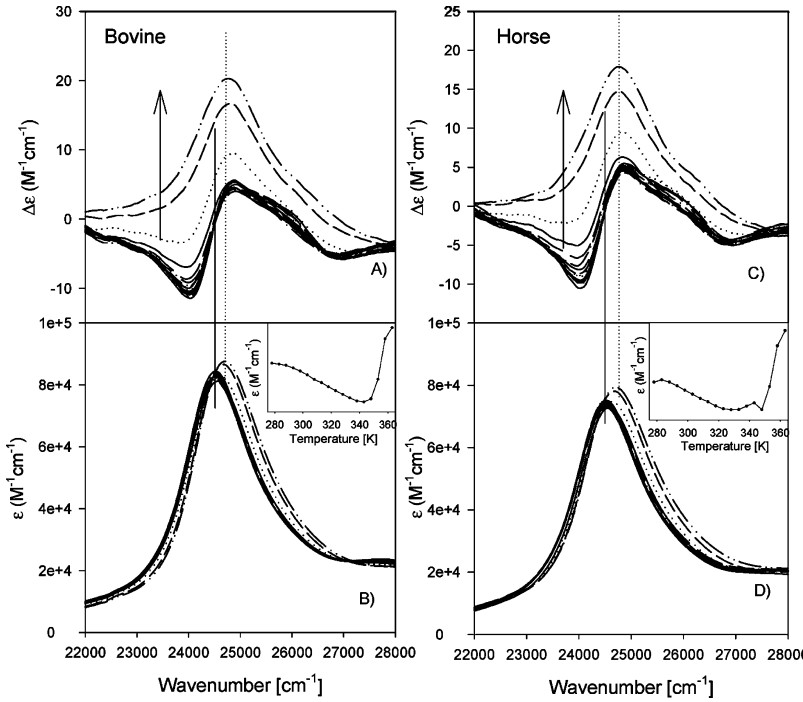

FIGURE 1: Visible circular dichroism (A and C) and absorption (B and D) spectra of bovine (left column) and horse heart ferricytochrome *c* (right column) taken at pH 7 in a Tris HCl buffer between 278 and 363 K in increments of 5 K. The arrows in these and all subsequent figures indicate the spectral changes with increasing temperature. The solid vertical line indicates maximum absorption frequency position at low temperature and dotted line indicates maximum absorption frequency at high temperature. Inset: ε vs temperature at the maximum absorption frequency. Spectra taken at temperatures between 278 and 348 K are plotted as solid lines; spectra taken at 353, 358 and 363 K are plotted as dotted, dashed, dashed-dotted line.

show different temperature dependences. $\Delta\varepsilon_{min}$ increases and $\Delta\varepsilon_{max}$ decreases with rising temperature below 343 K, which yields the more symmetric couplet at higher temperatures. All values sharply increase above 343 K, reflecting the cooperativity of the unfolding process. Thus, our data suggest a similar melting temperature for both proteins, but the slope of $\Delta\varepsilon$(T) is clearly steeper for hhc, indicating a higher degree of cooperativity. This result seems to be at variance with results from recent IR spectroscopic investigations of the thermal unfolding of horse heart and bovine ferricytochrome *c*, which suggest different unfolding mechanisms for the two proteins (*30*). For horse heart cytochrome *c*, Filosa et al. proposed a sequential unfolding of protein domains (in agreement with work from the Englander group (*33*)), whereas the data for bovine cytochrome *c* were interpreted as indicating a more global, cooperative unfolding (*15, 30, 32*). However, our data are likely to reflect the specific secondary and tertiary structure of the heme environment rather than global changes of the protein.

The data in Figures 1 and 2 indicate only modest spectral (and thus also structural) changes in the temperature region between 320 and 340 K, with which the thermal intermediate, III_h, is generally associated. However, the temperature dependencies of ε and $\Delta\varepsilon$ values exhibited in Figures 1 and 2, respectively, clearly indicate the population of an intermediate in the temperature region where III_h is generally populated. To check whether this state really resembles the well-known characteristics of the III_h state, we also measured the temperature dependence of absorption and ECD profile of the charge transfer band at 695 nm between 278 and 348 K, which are exhibited in Figure 3. The data clearly reveal the decrease of this band's intensity above 310 K (Figure 3 inset) as first observed by Schejter and George (*16*), which is generally viewed as characteristic for a III $\rightarrow$ III_h transition. Altogether, these findings suggest that III_h is thermodynamically distinct from state IV, since the latter cannot be significantly populated at the chosen experimental conditions.

Most of the investigations of the III $\rightarrow$ III_h transition have thus far been performed at neutral pH with a temperature-dependent buffer (*5, 15, 30, 32*). The question arises whether state III_h or IV is populated at higher temperatures, if a temperature-independent buffer with a low ionic strength is used. To address this issue, we measured the ECD and absorption spectra of the B-band in a buffer that remained at (nearly) constant pH as a function of temperature. This experiment was achieved by using a 1 mM MOPS (3-(*N*-morpholino)propanesulfonic acid) buffer. This buffer has a temperature coefficient of -1.3×10^{-3} pH units per °C. The low ionic strength of the corresponding solution ensured a rather low effective p*K*-value of the alkaline transition ($\sim$9 at room temperature and 8 in III_h region). The corresponding spectra are shown in Figure S1, Supporting Information. Apparently, the ECD spectrum and its temperature dependence are qualitatively very similar to what we obtained by using a Tris HCl buffer to decrease the pH while increasing the temperature. This notion is corroborated by the respective $\Delta\varepsilon(T)$ plots in Figure 4. Quantitatively, the two sets of spectra (Figures 1, left side, and Figure S1) differ slightly, which can be attributed to the anion concentrations used for the two experiments (*34*). Our data thus far indicate that the non-native states populated at pH 7 and 6 in the III_h temperature region are identical.

An earlier attempt to probe the thermal transitions of oxidized horse heart cytochrome *c* by ECD deserves to be mentioned in this context. Myer reported a change of Soret band ellipticity to occur at 313 K, which is not reproduced

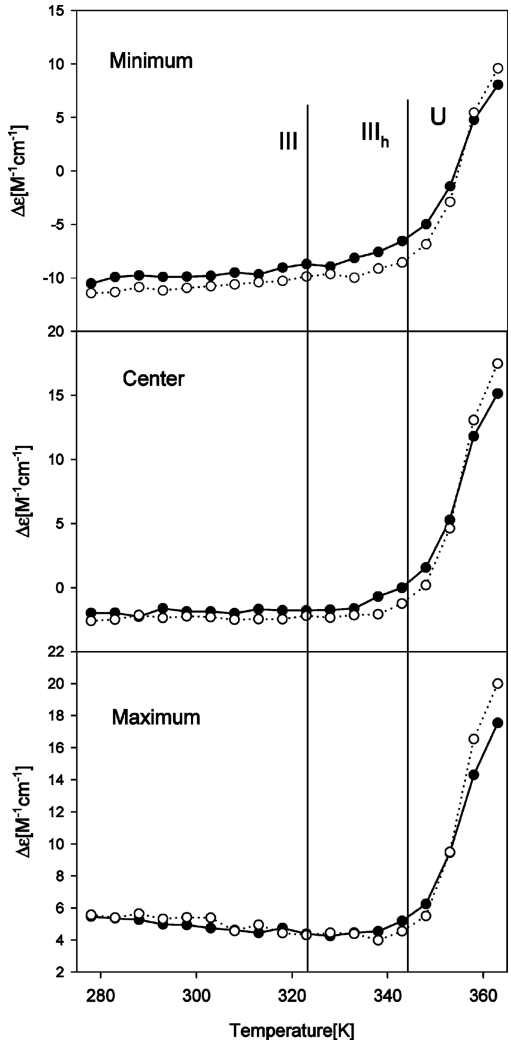

FIGURE 2: $\Delta\varepsilon$ vs temperature of bovine heart (open circles) and horse heart (closed circles) ferricytochrome *c* between 278 and 363 K measured in pH 7 Tris HCl buffer. The upper panel is at 24010 cm^{-1}, the middle is at 24450 cm^{-1}, and the lower is at 24876 cm^{-1}, corresponding to the minimum, the center and the maximum position of the B-band couplet at room temperature. The temperature regimes of the three states III, III_h and U (unfolded) are indicated.

by any of our data (neither for bovine nor for horse heart) (*21*). An inspection of his visible ECD spectra shows a disappearance of the couplet already at 333 K. An explanation for the observed data was not provided. We have no explanation for this discrepancy, but it should be noted that Myer did not use a buffer for his protein solution.

Secondary Structure Analysis of III_h by UV-ECD Measurements. We used far-UV ECD spectroscopy to probe secondary structure changes associated with the transition between different III-states. Far UV-ECD spectra recorded in the temperature range used for the visible-ECD measurements are consistent with the two melting phases reported for horse heart ferricytochrome *c* by Myer (*21*). Figure 5 shows the $\Delta\varepsilon$ value of bhc measured at 218 nm (44964 cm^{-1}) in 0.1 M Tris HCl buffer as a function of temperature. The onset of the first phase is at 323 K, while the second one starts at 343 K. The first phase can be assigned to the III → III_h transition and the second one to the melting of most of the secondary structure. These data add further support to

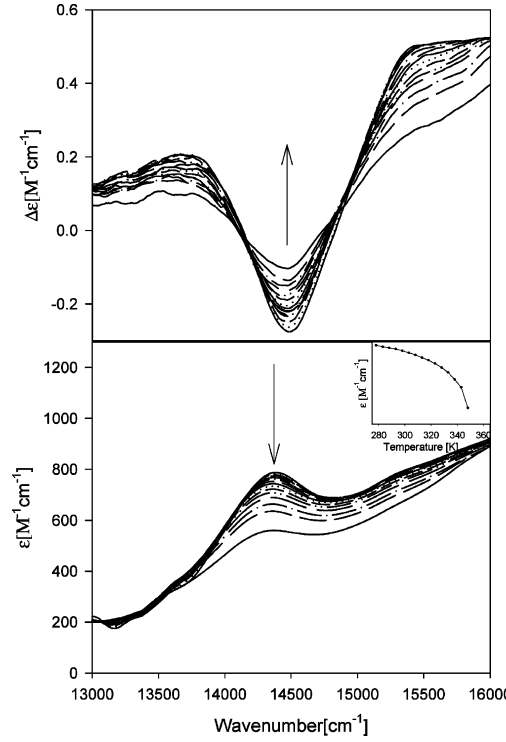

FIGURE 3: Temperature-dependent ECD (top) and absorption (bottom) spectra of bovine heart cytochrome *c* measured in the charge-transfer band region from 13000 to 16000 cm^{-1}. The spectra were measured in a pH 7 Tris HCl buffer with a 5 mM concentration. Inset: ε vs temperature at the maximum absorption frequency.

the notion that the III → III_h transition takes place at pH values well below the p*K* value of the alkaline transition.

To quantitatively probe secondary structure changes associated with the III → III_h transition we performed far-UV ECD experiments using the synchrotron radiation (SR) source at Brookhaven National Laboratories. Thus, we obtained ECD spectra in a wavelength range between 170 and 260 nm, which allow for a more reliable secondary structure analysis than ECD spectra taken with a conventional instrument. SRCD spectra were taken at 296 K and 345 K (Figure 6). The spectra were processed with the spectral processing program CDTools (*35*) and analyzed with the secondary structure from circular dichroism spectroscopic data program, Dichroweb (*36, 37*), using the program ContinLL and reference set 1. This analysis yielded approximately a 15% loss of α-helical content, redistributed to mostly extended and to a minor extent turn and unordered structures at 345 K (state III_h) compared with 296 K (III). Hence, state III_h is partially unfolded rather than a classical molten globule state.

Interpretation of Visible ECD and Absorption Spectra. A more thorough understanding of the above-reported ECD spectra requires a comparison with the respective absorption spectra. The spectra in Figures 1 and 4 reveal that the peak of B-band absorption is situated between the couplet extrema at temperatures below 343 K. At higher temperatures, however, the peak coincides with the maximum of the Cotton band. This result indicates that the B-band is split into its B_x and B_y components below 343 K, owing to electronic and vibronic perturbations imposed by the protein environment (*28, 29*).

We used a recently developed vibronic coupling model (*29*) to simulate three ECD spectra of bovine cytochrome *c* (in Tris HCl buffer), recorded at 278, 338 (data not shown)

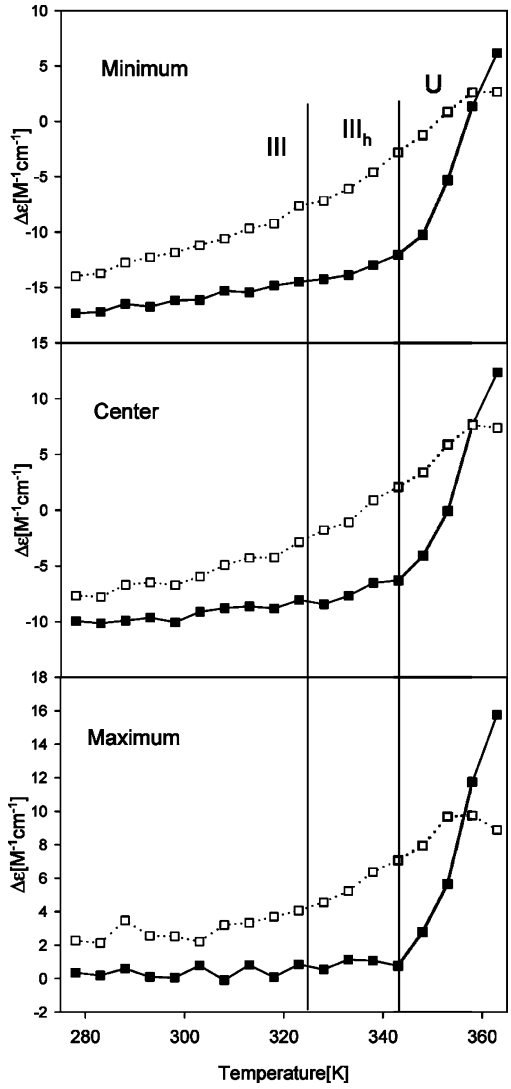

FIGURE 4: Δε vs temperature of bovine heart pH 7.0 (closed squares) and bovine heart pH 8.5 (open squares) ferricytochrome *c* between 278 and 363 K measured in MOPS buffer. The upper panel is at 24010 cm^{-1}, the middle is at 24450 cm^{-1}, and the lower is at 24876 cm^{-1}, corresponding to the minimum, the center and the maximum position of the B-band couplet at room temperature. The temperature regimes of the three states III, III$_h$ and U (unfolded) are indicated.

and 363 K (simulations shown in Figure 7). Since the oxidation marker band ν_4 dominates the resonance Raman spectrum for excitations of the B-band region (data not shown), we considered only the contribution of this mode to the vibronic sideband. This model is a simplification, but it is sufficient for exploring the amount of splitting. The general theory of the model is described in ref *29*, so we confine ourselves here to presenting the most relevant equations and some modifications. If one neglects coupling between $|B_x\rangle$ and $|B_y\rangle$ states, the energy eigenvalues associated with the $0 \rightarrow 0$ transition are written as

$$E^{B'}_{l,0} = E^{B}_{l,0} - \sum_{\Gamma''} \frac{\left[c^{\Gamma''}_{B_l B_l}(\nu_4)\right]^2}{\Omega^{B}_{\nu_4}} \qquad (1)$$

where $E^{B'}_{l,0}$ ($l = x, y$) denotes the eigenenergies of the vibronically and electronically perturbed B-state and $E^{B}_{l,0}$ are the energies of the electronically perturbed states $|B_l,0\rangle$. $\Omega^{B}_{\nu_4}$ denotes the vibrational energies of the ν_4 vibration in the excited

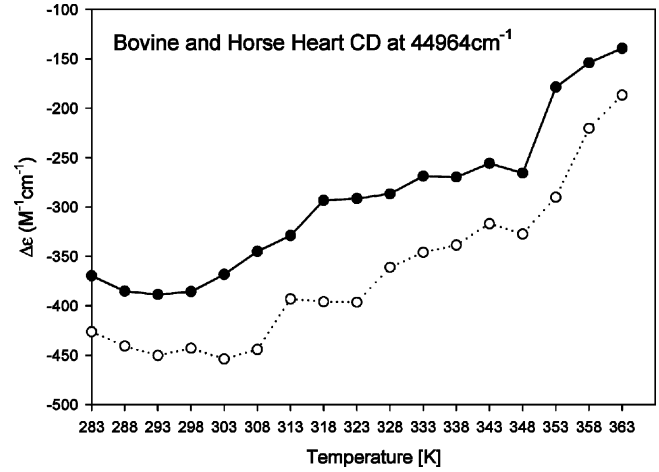

FIGURE 5: Δε of bovine (closed circles) and horse heart (open circles) ferricytochrome *c* as a function of temperature at 44964 cm^{-1} in the far UV region with a pH 7 Tris HCl buffer.

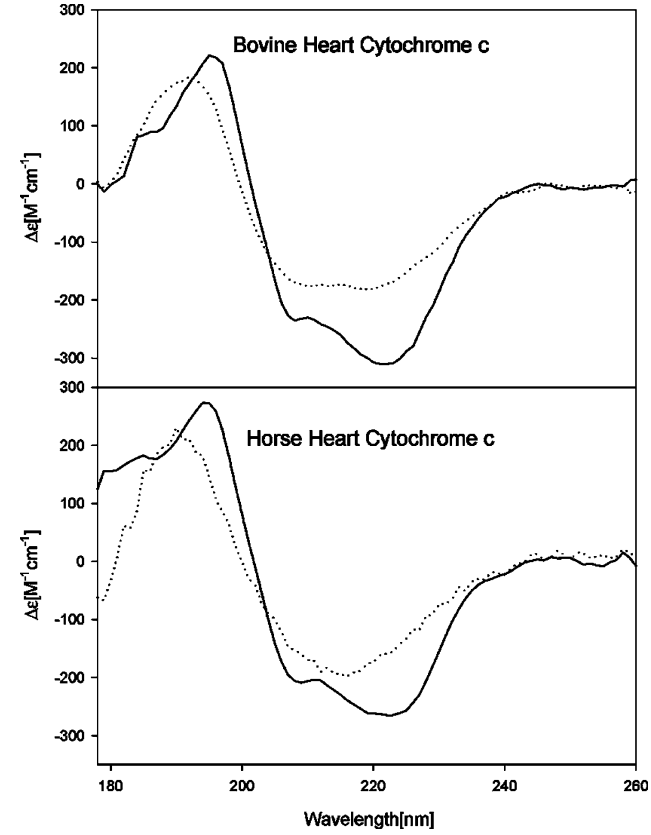

FIGURE 6: Temperature-dependent far-UV SRCD spectra of bovine (top) and horse (bottom) heart ferricytochrome *c*. Solid line: 296 K. Dotted line: 345 K.

B-states. The parameter $c^{\Gamma''}_{e,s}(\nu_4)$ (e, $s = B_l$) denotes the corresponding vibronic coupling matrix element. Γ' is the effective symmetry of the respective vibration in the presence of symmetry lowering perturbations. The second term on the right of eq 1 describes the contribution from intrastate Franck−Condon (A_{1g}) and Jahn−Teller (B_{1g}, B_{2g}) coupling associated with the ν_4 mode, which is totally symmetric in ideal D_{4h}. The pure electronic eigenenergies, $E^{B}_{x,0}$ and $E^{B}_{y,0}$ are identical in D_{4h}, but are split in a protein environment. The total electronic splitting of the B_0 is written as (*38*)

$$\Delta E^{B} = \Delta_{Stark} + \frac{2\delta^{A_{1g}}_{QB}\delta^{B_{1g}}_{QB}}{E^{B_0} - E^{Q_0}} \qquad (2)$$

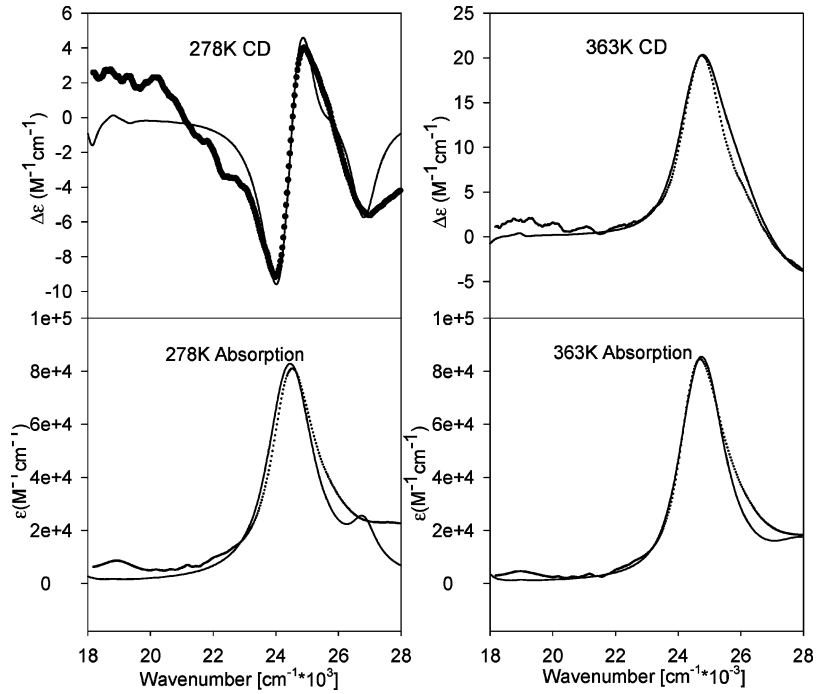

FIGURE 7: Experimental (dots) and simulated (solid line) ECD (upper panel) and absorption spectra (lower panel) of bovine heart ferricytochrome *c*. The experimental spectra were measured at the indicated temperatures.

where δ_{QB}^{A1g} and δ_{QB}^{B1g} describe electronic perturbations of A_{1g} and B_{1g} symmetry. The latter is assigned to the quadrupole moment of the internal electric field. These perturbations cause a mixing of Q- and B-states and an equal splitting of their energies. Δ_{Stark} denotes the different shifts of B_x and B_y, owing to a quadratic Stark effect, which mixes the ground-state with both components of the excited B-state (*31*). Since the Stark splitting scales with the square of the corresponding transition dipole moment, it is much larger for the B- than for the Q-band. The electronic part of the Q-band splitting can be nearly exclusively assigned to the electric field's quadrupole moment (*31, 39*).

As mentioned above, the vibronic sideband B_v is modeled as mainly resulting from the vibronic coupling of ν_4. This is a rather crude approximation of the vibronic sideband. The respective transition dipole moments (electronic and magnetic) $\vec{\pi}^{B}_{l,1_{\nu 4}}$ are described by the equation:

$$\vec{\pi}^{B}_{l,1_{\nu 4}} = \frac{c^{\Gamma''}_{B_l B_l}(\nu_4)}{\Omega^{B}_{\nu_4}} \vec{\pi}^{B}_{l,1_{\nu 4}} \qquad (3)$$

Figure 7 compares experimental data and simulation for the spectra recorded at 278 and 363 K. The simulation for the 338 K spectra is of similar quality. This analysis yielded an identical splitting of 360 cm^{-1} for 278 and 338 K (data not shown), whereas the splitting is practically zero for the 363 K measurement. Interestingly, our splitting value is only slightly larger than what Manas et al. observed for the B-band in the low temperature spectrum of Zn-substituted horse heart cytochrome *c* (296 cm^{-1}) (*40*). Compared with the low temperature spectrum, the rotational strength values for B_x and B_y at 338 K are reduced by factors of 0.81 and 0.76, respectively. At 363 K the amount of the total rotational strength is increased by a factor of 1.6 compared to the corresponding value obtained for 338 K. The splitting most likely provides us with a lower limit for the electronic perturbation energy, since vibronic perturbations, which are not fully accounted for at the present level of analysis, generally reduce, rather than increase, the splitting (*38*).

Our experimental data suggest that the B-state electric field strength in the heme plane is not significantly changed by the III → III_h transition. The concomitant decrease of the rotational strength for B_x and B_y might reflect a reduction of out-of-plane deformations, which have been shown to cause substantial rotational strength of opposite sign for both B-band transitions (*41*). Additionally, invoked orientational changes of aromatic residues in the heme pocket (e.g., F82) certainly contribute to the rotational strength (*26*). Specific site-directed mutations experiments are necessary to clarify this issue. A final assessment of the B-band's Stark effect has recently been made by virtue of a full vibronic analysis of the Q- and the B-band splitting of ferri- and ferrocytochrome *c* (*42*).

The absence of any detectable splitting in the ECD spectra of bhc in the unfolded states and, as shown below, in states IV and V seems to suggest an absence of a quadratic Stark effect. This hypothesis is unlikely for a variety of reasons. First, our spectra indicate that the heme is still bound to the protein in these states. It is therefore likely that the protein still produces an electric field in the heme plane. Moreover, a substantial decrease of the electric field would cause a significant redshift of both Q- and B-band (*31*), which is not observed. The absence of splitting can be rationalized in terms of a compensation of vibronic and electronic perturbations, which generally have opposite signs for the Q-band. Alternatively, one may invoke larger protein fluctuations as giving rise to a distribution of different orientations of the electric field with respect to the heme plane. If this distribution is nearly symmetric with respect to one of the C_mFeC_m of the heme macrocycle, the effective electronic splitting could be very small, even though the electric field is still rather strong (*31, 42, 43*).

It is necessary in this context to point out that the interpretations of visible CD spectra of heme proteins are often too simplistic. The absence of the B-band couplet in spectra of yeast-cytochrome *c* mutants, in which F82 is replaced by another residue (*44*), cannot be interpreted as indicating that the negative component of the couplet arises from coupling between the heme and the phenylalanine ring (*45*). On the contrary, since phenylalanine is aromatic and hydrophobic, its contribution to the internal field is very small. By the same token, it is incorrect to assign the substitution of a couplet by a single, positive Cotton band to a disruption of the coupling between the heme group and aromatic acid residue in the heme pocket (*46*). For hemoglobin and myoglobin (*26, 29*), single positive Cotton bands, were measured for the respective intact molecules. The absence of a couplet in the B-band regions can have several reasons. First, the band splitting is small and one component (*x* or *y*) has more rotational strength than the other one. This is most likely the case for the above-discussed thermally unfolded state of cytochrome *c*. That this is possible has been shown by Blauer et al. (*41*). Second, it is possible that only one of the two components carries substantial rotational strength. If the band is split, this can lead to a positive (or negative) Cotton band, the wavenumber position of which does not coincide with that of the respective absorption band. As recently shown, this is the case in deoxymyoglobin and myoglobin cyanide (*29*).

Characterizing the Alkaline States. The results discussed thus far show that III_h and IV are thermodynamically distinct. The III → III_h transition state is generally associated with the disappearance of the 695 nm band, which is interpreted as reflecting the rupture of the Fe^{3+}−M80 bond (*5, 16*). This is certainly the case for state IV, but the data displayed in Figure 3 suggest a decrease of the 695 nm band's oscillator strength rather than its disappearance in III_h. This notion is strongly corroborated by the still significant rotational strength of the band in the III_h temperature region. We therefore infer that III_h differs structurally from IV-states in that the Fe^{3+}−M80 bond, even though weakened, is still present in the former. This notion is consistent with the above-discussed similarity of the ECD spectra of III and III_h. To explain possible structural differences, we measured the temperature dependence of the B-band (ECD and absorption) of bhc at pH 8.5 and 10.5. The respective pH values were adjusted by adding NaOH to a 1 mM MOPS buffer solution for the former and to a 50 mM Bis/Tris buffer solution for the latter. Figure S2, Supporting Information, depicts the spectra measured at pH 8.5. The corresponding insets exhibit the temperature dependence of ε_{max}. The couplet observed at low temperatures converts to a positive Cotton band at significantly lower temperatures (333 K) than the couplets obtained at neutral (Figure S1) and (slightly) acidic pH (Figure 1). Figure 8 compares the temperature dependence of both $\Delta\varepsilon$ and the Kuhn anisotropy, measured at pH 8.5 with the respective data recorded with solution exhibiting pH 7 at room temperature. The rather smooth temperature dependencies of $\Delta\varepsilon$ and $\Delta\varepsilon/\varepsilon$ recorded at pH 8.5 stretch over the entire temperature range investigated, thus indicating a noncooperative transition between a low and high temperature state, which, based on the respective ECD spectra, resemble III_h and U. However, a two-state transition is ruled out by the absence of an isodichroic point and by the

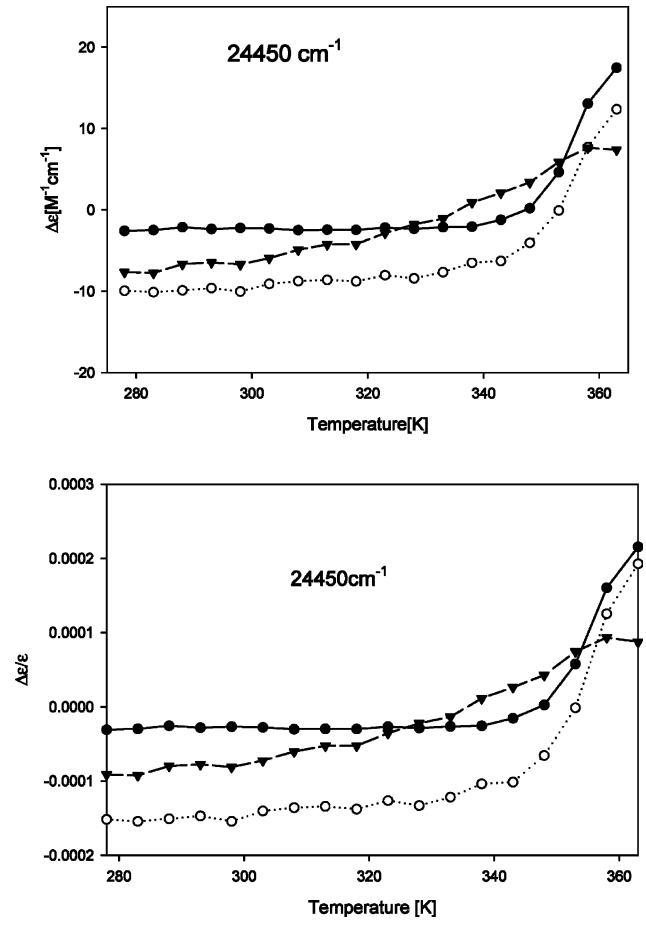

FIGURE 8: (Top) $\Delta\varepsilon$ vs temperature and (bottom) Kuhn anisotropy, $\Delta\varepsilon/\varepsilon$, vs temperature at the indicated frequency position of pH 7 (tris buffer) bhc (open circles), pH 7 (MOPS buffer) bhc (closed circles) and pH 8.5 (MOPS buffer) bhc (triangles), between 278 and 363 K.

corresponding nonmonotonous temperature-dependence of ε_{max} (inset Figure S2), which exhibits a pronounced minimum at 310 K. At this temperature the effective p*K*-value of the alkaline transition is nearly identical with the adjusted pH of 8.5 (*19*), so that the minimum coincides with the half-point of the III → IV transition. It should be noted that the CD spectra in Figure S2 bear some resemblance with the aforementioned spectra reported by Myer, which might indicate that his actual pH was slightly basic (*21*).

More information about state(s) IV can be inferred from the ECD (and absorption) profiles measured at pH 10.5, which are exhibited in Figure S3, Supporting Information. At this pH the alkaline state(s) IV are predominantly populated even at room temperature. The corresponding ECD spectra already show a positive Cotton band in the Soret region, which is quite distinct from the symmetric couplet observed for the III_h state. The rotational strength increases with increasing temperature while the absorption peak exhibits a redshift, in contrast to what was observed for the III_h → U transition at neutral and modestly acidic pH. The positive Cotton band and its coincidence with the absorption maximum reflect again the drastically reduced splitting between the B_x and B_y bands. Figure 9 exhibits the corresponding temperature dependence of $\Delta\varepsilon_{max}$. Additionally, the respective Kuhn anisotropies (*47*), $\Delta\varepsilon/\varepsilon$, are plotted in Figure 9. While $\Delta\varepsilon_{max}$ seems to be nearly temperature independent between 278 and 338 K within the experimental uncertainty

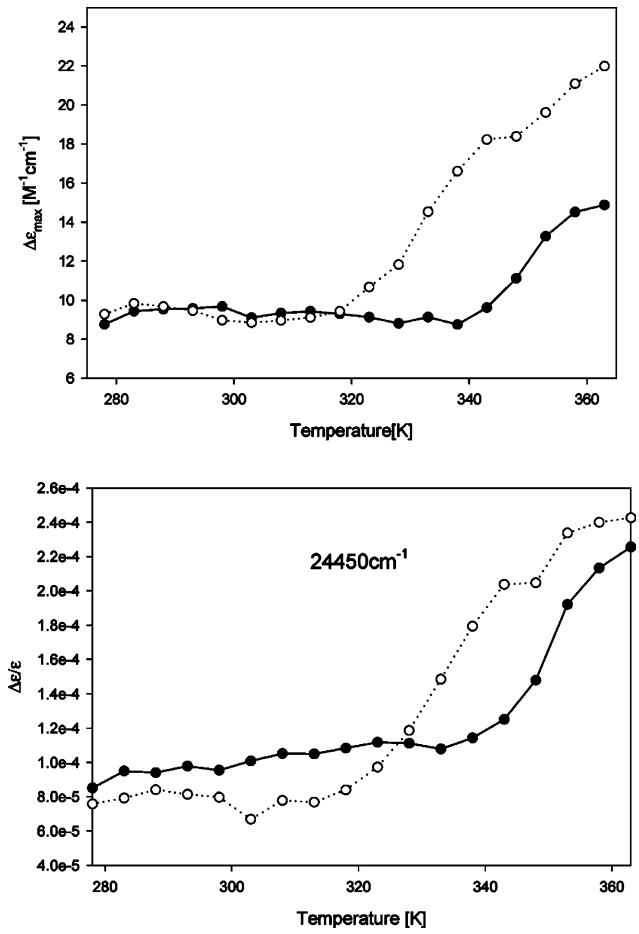

FIGURE 9: (Top) $\Delta\varepsilon_{max}$ vs temperature and (bottom) Kuhn anisotropy, $\Delta\varepsilon/\varepsilon$, vs temperature at the indicated frequency position of pH 10.5 (bis/tris buffer) bhc (closed circles) and pH 11.5 (bis/tris buffer) bhc (open circles) between 278 and 363 K.

(i.e., 6%), the Kuhn anisotropy exhibits a statistically significant though small increase with rising temperature. Both $\Delta\varepsilon_{max}$ and Kuhn anisotropy exhibit a steep increase with increasing temperatures above 348 K. The data indicate the existence of at least two thermal transitions, involving an intermediate IV_h and a certainly unfolded state IV_u. Apparently, the rotational strength is significantly larger at pH 10.5 than at 8.5 and at lower pH values for the entire temperature range. This indicates that at pH 8.5 state IV still coexists with other states (III_h or some yet unidentified state) even at high temperatures. The interpretation of the data at this pH is complicated by the possible coexistence of most likely three alkaline isomers and also by the fact that the (lysine) protonation and the dissociation of M80 are thermodynamically distinct processes (*11*).

To gain a complete picture of the conformational manifold sampled at alkaline pH we also measured the temperature dependence of the ECD and absorption spectra of bhc at pH 11.5. The alkaline state, V, can be expected to be populated at room temperature at this pH (*9*). The ECD spectra in Figure S4, Supporting Information (pH 11.5), are qualitatively similar to those obtained at pH 10.5 in that they start as a positive Cotton band as well and, like the spectra in Figure S3, increase with increasing temperature. However, the corresponding spectra (Figure S4) are quantitatively different from that observed in Figure S3. The magnitude of this difference can be seen by comparing plots in Figure 9, where the associated $\Delta\varepsilon_{max}$ are plotted as a function of temperature. The maximal dichroism of the Cotton band representing state IV is smaller than that of state V at temperatures above 320 K. The respective temperature dependences of the ε_{max} values are also significantly different. The maximal extinction decreases nearly monotonously with increasing temperature for state IV (Figure S3). For state V, ε_{max} first increases to reach a plateau at 330 K, from where it decreases further to a minimum at 350 K. Upon increasing the temperature further, ε_{max} increases dramatically. On the contrary, the Kuhn anisotropy increases already above 320 K. It reaches a plateau at 340 K and increases only slightly at higher temperatures. The data clearly indicate that the melting of state V involves at least two intermediates which exhibit significantly different ε_{max} and slightly different $\Delta\varepsilon_{max}$ values. The unfolded states of IV and V exhibit similar Kuhn anisotropies, but the rather different ε_{max} and $\Delta\varepsilon_{max}$ values suggest that this coincidence is accidental. It should be noted that the population of the unfolded V state causes a dramatic upshift of the Soret band (Figure S4), which was not observed for the unfolded state of IV (Figure S3).

For comparative purposes, Figure 10 depicts the differences of the ECD and absorption spectra of bhc, which reflect the aforementioned native and non-native conformations. The low-temperature spectra represent the states III−V. Spectra taken at the indicated intermediate temperature can at least partially be assigned to the corresponding thermal intermediates, and the spectra taken at high temperature reflect the corresponding unfolded state. At room temperature, the ECD spectra obtained in state III (pH 7 and 8.5) display couplets in the Soret region with the peak extinctions situated in the middle of the couplet. The higher pH measurements in states IV (pH 10.5) and V (pH 11.5) display positive Cotton bands at room temperature, though the intensity of the band in state V is much larger than any of the other investigated states. At high temperature all of the ECD profiles turn into positive Cotton bands and become (nearly) coincident with their respective absorption profiles. However, in terms of absolute rotational strength, band shapes and absorptivity, the bands assignable to the unfolded states of III, IV and V are different, thus indicating that these states are not structurally identical in the vicinity of the heme group. In what follows we term these states III_u, IV_u and V_u.

We deduce the following minimal thermodynamic scheme from our data:

$$\begin{array}{ccccc} III_u & \Leftrightarrow & IV_u & \Leftrightarrow & V_u \\ & & & & \Updownarrow \\ \Updownarrow & & \Updownarrow & & V_{h2} \\ & & & & \Updownarrow \\ III_h & \Leftrightarrow & IV_h & \Leftrightarrow & V_{h1} \\ \Updownarrow & & \Updownarrow & & \Updownarrow \\ III_n & \Leftrightarrow & IV_n & \Leftrightarrow & V_n \end{array}$$

The further characterization of the newly identified conformations is currently underway in our laboratory. We wish to reiterate in this context that state IV, and to some extent also state III, encompasses conformational substates with different axial ligands (for IV) (*11*) or different Fe^{3+}−M80 bonding strengths (III) (*20, 34*).

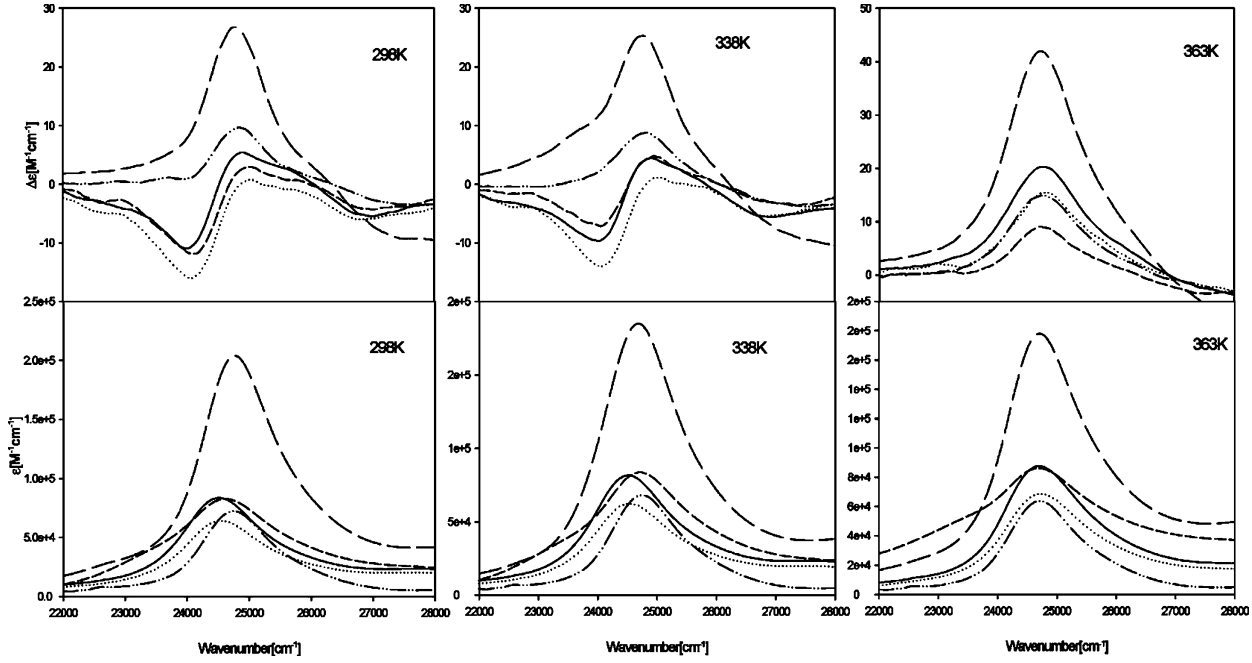

FIGURE 10: ECD (top) and absorption (bottom) of all investigated pH measurements (pH 7 Tris HCl buffer, solid line; pH 7.0 MOPS buffer, dotted line; pH 8.5 MOPS buffer, short dashed line; pH 10.5 Bis/Tris buffer, dashed-dot-dot line; and pH 11.4 Bis/Tris buffer, long dashed line) of bovine heart cytochrome *c* at room temperature (left panels), intermediate temperature (middle panels) and high temperature (right panels). Exact temperatures are indicated in individual panels.

One would naively expect that the rotational strength of a heme band decreases upon thermal unfolding. Our data indicate, however, that not only $\Delta\varepsilon_{max}$ but also the integrated rotational strength increases, as does the Kuhn anisotropy. Since $\Delta\varepsilon/\varepsilon \propto \vec{m}_B \cdot \cos(\vec{\mu}_B, \vec{m}_B)/\vec{\mu}'_B)$, with $\vec{m}_B$ as the magnetic and $\vec{\mu}'_B$ as the electronic matrix element of the transition into the B-states, our data are indicative of a substantial increase of a magnetic dipole component in the heme plane. Since the latter arises from heme−protein interactions (*26*), our data thus indicate an increase of some electronic coupling between the heme and protein chromophores in non-native states, which contradicts the notion of reduced heme−protein coupling in unfolded states.

SUMMARY

Taken together, this article demonstrates how visible ECD and absorption spectroscopy can be used to elucidate differences between native, non-native, thermally populated intermediates and thermally unfolded states of ferricytochrome *c* by a spectral comparison with carefully defined parameters, i.e. buffer conditions and ionic strength. The extent of band splitting caused by electrostatic interactions between the heme group and the protein was determined by a vibronic analysis of the B-band's ECD and absorption spectrum. We demonstrated that the states III_h and IV are thermodynamically and also conformationally different, contrary to the current belief. With respect to ferricytochrome *c* our results suggest that the overall structure is maintained in the intermediate state populated above 323 K. Conformational changes might involve increasing distances between the heme and aromatic residues such as F82 and a reduced nonplanarity of the heme macrocycle. The band splitting is substantially reduced in the unfolded states, but the heme environment encompassing H18 and the two cysteine residues 14 and 17 is most likely still intact and covalently bound to the heme chromophore. Most importantly, this work exemplifies the need for a comprehensive thermodynamic analysis of all native and non-native states of ferricytochrome *c* under well-defined conditions which would explicitly consider the fact that not only the "ground state" populated at room temperature but also the thermally excited, partially or mostly unfolded states are still pH dependent.

ACKNOWLEDGMENT

We would like to acknowledge John Trunk at Brookhaven National Laboratories for his assistance recording the SRCD spectra.

SUPPORTING INFORMATION AVAILABLE

Figures S1−S4 exhibit ECD spectra measured at pH 7, 8.5, 10.5 and 11.5. This material is available free of charge via the Internet at http://pubs.acs.org.

REFERENCES

1. Moore, G. W., and Pettigrew, G. W. (1990) *Cytochrome c 194 evolutionary, structural and physicochemical aspects*, Springer, Berlin, Heidelberg, New York.
2. Liu, X., Kim, C. N., Yang, J., Jemmerson, R., and Wang, X. (1996) Induction of apoptotic program in cell-free extracts: requirement for dATP and cytochrome c. *Cell 86*, 147–157.
3. Jemmerson, R., Liu, J., Hausauer, D., Lam, K-P., Mondino, A., and Nelson, R. D. (1999) A conformational change in cytochrome c of apoptotic and necrotic cells is detected by monoclonal antibody binding and mimicked by association of the native antigen with synthetic phospholipid vesicles. *Biochemistry 38*, 3599–3609.
4. Belikova, N. A., Vladimirov, Y. A., Osipov, A. N., Kapralov, A. A., Tyurin, V. A., Potapovich, M. V., Basova, L. V., Peterson, J., Kurnikov, I. V., and Kagan, V. E. (2006) Peroxidase activity and structural transitions of cytochrome c bound to cardiolipin-containing membranes. *Biochemistry 45*, 4998–5009.
5. Taler, G., Schejter, A., Navon, G., Vig, I., and Margoliash, E. (1995) The nature of the thermal equilibrium affecting the iron coordination of ferric cytochrome c. *Biochemistry 34*, 14209–14212.
6. Kluck, R. M., Ellerby, L. M., Ellerby, H. M., Naiem, S., Yaffe, M. P., Margoliash, E., Bredesen, D., Mauk, G., Sherman, F., and

Newmeyer, D. M. (2000) Determinants of cytochrome c pro-apoptotic activity. The role of lysine 72 trimethylation. *J. Biol. Chem. 275*, 16127–16133.
7. Dyson, H. J., and Beattie, J. K. (1982) Spin state and unfolding equilibria of ferri-cytochrome c in acidic solution. *J. Biol. Chem. 257*, 2267–2273.
8. Goto, Y., Takahashi, N., and Fink, A. L. (1990) Mechanism of Acid-Induced Folding of Proteins. *Biochemistry 29*, 3480–3488.
9. Döpner, S., Hildebrandt, P., Rosell, F. I., and Mauk, A. G. (1998) The alkaline conformational transitions of ferricytochrome c studied by resonance Raman spectroscopy. *J. Am. Chem. Soc. 120*, 11246–11255.
10. Rossel, F. I., Ferrer, J. C., and Mauk, A. G. (1998) Proton-linked protein conformational switching: definition of the alkaline conformational transition of yeast iso-l-ferricytochrome c. *J. Am. Chem. Soc. 120*, 11234–11245.
11. Blouin, C., Guillemette, J. G., and Wallace, C. J. A. (2001) Resolving the individual components of a pH-induced conformational change. *Biophys. J. 81*, 2331–2338.
12. Döpner, S., Hildebrandt, P., Rosell, F. I., Mauk, A. G., von Walter, M., Soulimane, T., and Buse, G. (1999) The structural and functional role of lysine residues in the binding domain of cytochrome c for the redox process with cytochrome c oxidase. *Eur. J. Biochem. 261*, 379–391.
13. Kumar, R., Prabhu, N. P., Rao, D. K., and Bhuyan, A. K. (2006) The alkali molten globule state of horse ferricytochrome c: Observation of cold denaturation. *J. Mol. Biol. 364*, 483–495.
14. Sagle, L. B., Zimmermann, J., Dawson, P. E., and Romesberg, F. E. (2006) Direct and high resolution characterization of cytochrome C equilibrium folding. *J. Am. Chem. Soc. 128*, 14232–14233.
15. Filosa, A., and English, A. M. (2000) Probing local thermal stabilities of bovine, horse, and tuna ferricytochromes c at pH 7. *JBIC, J. Biol. Inorg. Chem. 4*, 448–454.
16. Schejter, A., and George, P. (1964) The 695 mμ band of ferricytochrome c and its relationship to protein conformation. *Biochemistry 3*, 1045–1049.
17. Barker, P. D., and Mauk, A. G. (1992) pH-Linked conformational regulation of a metalloprotein oxidation-reduction equilibrium: electrochemical analysis of the alkaline form of cytochrome c. *J. Am. Chem. Soc. 114*, 3619–3624.
18. Battistuzzi, G., Loschi, L., Borsari, M., and Sola, M. (1999) Effects of nonspecific ion-protein interactions on the redox chemistry of cytochrome c. *JBIC, J. Biol. Inorg. Chem. 4*, 601–607.
19. Battistuzzi, G., Borsari, M., Loschi, L., Martinelli, A., and Sola, M. (1999) Thermodynamics of the alkaline transition of cytochrome c. *Biochemistry 38*, 7900–7907.
20. Schweitzer-Stenner, R., Shah, R., Hagarman, A., and Dragomir, I. (2007) Conformational substates of horse heart cytochrome c exhibit different thermal unfolding of the heme cavity. *J. Phys. Chem. B 111*, 9603–9607.
21. Myer, Y. P. (1968) Conformation of cytochromes. III. Effect of urea, temperature, extrinsic ligands and pH variation on the conformation of horse heart ferricytochrome-c. *Biochemistry 7*, 765–776.
22. Myer, Y. P., and Harbury, H. A. (1966) Optical rotatory dispersion of cytochrome c II. Comparative data for a heme octapeptide. *J. Biol. Chem. 241*, 4299–4303.
23. Urry, D. W., and Doty, P. (1967) *J. Am. Chem. Soc. 87*, 2756.
24. Urry, D. W. (1965) Protein-heme interactions in heme-proteins: cytochrome C. *Proc. Natl. Acad. Sci. U.S.A. 54*, 640–648.
25. Drucker, H., Campbell, L. L., and Woody, R. W. (1970) Optical rotary properties of the cytochrome c_8 species of *Desulfovibrio*. *Biochemistry 9*, 1519–1527.
26. Hsu, M. C., and Woody, R. W. (1971) The origin of the heme cotton effects in myoglobin and hemoglobin. *J. Am. Chem. Soc. 93*, 3515–3525.
27. Kiefl, C., Sreerama, N., Haddad, R., Sun, L., Jentzen, W., Lu, Y., Qiu, Y., Shelnutt, J. A., and Woody, R. W. (2002) Heme distortions in sperm-whale carbonmonoxy myoglobin: correlations between rotational strengths and heme distortions in MD-generated structures. *J. Am. Chem. Soc. 124*, 3385–3394.
28. Dragomir, I., Hagarman, A., Wallace, C., and Schweitzer-Stenner, R. (2007) Optical band splitting and electronic perturbations of the heme chromophore in cytochrome c at room temperature probed by visible electronic circular dichroism spectroscopy. *Biophys. J. 92*, 989–998.
29. Schweitzer-Stenner, R., Gorden, J. P., and Hagarman, A. (2007) The asymmetric band profile of the soret band of deoxymyoglobin is caused by electronic and vibronic perturbations of the heme group rather than by a doming deformation. *J. Chem. Phys. 127*, 135103.
30. Filosa, A., Yang, Y., Ismail, A. A., and English, A. M. (2001) Two-dimensional infrared correlation spectroscopy as a probe of sequential events in the thermal unfolding of cytochromes c. *Biochemistry 40*, 8256–8263.
31. Manas, E. S., Vaderkooi, J. M., and Sharp, K. A. (1999) The effects of protein environment on the low temperature electronic spectroscopy of cytochrome c and microperoxidase-11. *J. Phys. Chem. B 103*, 6334–6348.
32. Filosa, A., Ismail, A. A., and English, A. M. (1999) FTIR-monitored thermal titration reveals different mechanisms for the alkaline isomerization of tuna compared to horse and bovine cytochromes c. *JBIC, J. Biol. Inorg. Chem. 4*, 717–726.
33. Krishna, M. M. G., Maity, H., Rumbley, J. N., Lin, Y., and Englander, S. W. (2006) Order of steps in the cytochrome c folding pathway: Evidence for a sequential stabilization mechanism. *J. Mol. Biol. 359*, 1410–1419.
34. Shah, R., and Schweitzer-Stenner, R. (2008) Structural changes of horse heart ferricytochrome c induced by changes of ionic strength and anion binding. *Biochemistry*, in press.
35. Lees, J. G., Smith, B., Wien, F., Miles, A., and Wallace, B. A. (2004) *CDtool*—An integrated software package for circular dichroism spectroscopic data processing, analysis and archiving. *Anal. Biochem. 332*, 285–289.
36. Whitmore, L., and Wallace, B. A. (2004) DICHROWEB, an online server for protein secondary structure analyses from circular dichroism spectroscopic data. *Nucleic Acids Res. 32*, W668−W673.
37. Lobley, A., Whitmore, L., and Wallace, B. A. (2002) DICHROWEB: An interactive website for the analysis of protein secondary structure from circular dichroism spectra. *Bioinformatics 18*, 211–212.
38. Schweitzer-Stenner, R., and Bigman, D. (2001) Electronic and vibronic contributions to the band splitting in optical spectra of heme proteins. *J. Phys. Chem. B 105*, 7064–7073.
39. Levantino, M., Huang, Q., Cupane, A., Laberge, M., Hagarman, A., and Schweitzer-Stenner, R. (2005) The importance of vibronic perturbations in ferrocytochrome c spectra: A reevaluation of spectral properties based on low-temperature optical absorption, resonance Raman, and molecular-dynamics simulations. *J. Chem. Phys. 123*, 054508.
40. Manas, E. S., Wright, W. W., Sharp, K. A., Friedrich, J., and Vanderkooi, J. M. (2000) The influence of protein environment on the low temperature electronic spectroscopy of Zn-substituted cytochrome c. *J. Phys. Chem. B 104*, 6932–6941.
41. Blauer, G., Sreerama, N., and Woody, R. W. (1993) Optical activity of hemoproteins in the soret region. circular dichroism of the heme undecapeptide of cytochrome c in aqueous solution. *Biochemistry 32*, 6674–6679.
42. Schweitzer-Stenner, R. (2008) The Internal Electric Field in Cytochrome C Explored by Visible Electronic Circular Dichroism Spectroscopy. *J. Phys. Chem. B*. [Online early access]. DOI: 10.1021/jp802495q. Published Online: July 30, 2008. http://pubs.acs.org/cgi-bin/asap.cgi/jpcbfk/asap/html/jp802495q.html.
43. Prabhu, N. V., Dalosto, S. D., Sharp, K. A., Wright, W. W., and Vanderkooi, J.M. (2002) Optical Spectra of Fe(II) Cytochrome c Interpreted Using Molecular Dynamics Simulations and Quantum mechanical Calculations. *J. Phys. Chem. B 106*, 5561–5571.
44. Pielak, G. J., Oikawa, K., Mauk, A. G., Smith, M., and Kay, C. M. (1986) Elimination of the Negative Soret Cotton Effect of Cytochrome c by Replacement of the Invariant Phenylalanine Using Site-Directed Mutagenesis. *J. Am. Chem. Soc. 108*, 2724–2727.
45. Indiani, C., de Sanctis, G., Neri, F., Santos, H., Smulevich, G., and Coletta, M. (2000) Effect of pH on Axial Ligand Coordination of Cytochrome c″ from *Methylophilus methylotrophus* and Horse Heart Cytochrome c. *Biochemistry 39*, 8234–8242.
46. Pinheiro, T. J. T., Elöve, G., Watts, A., and Roder, H. (1997) Structural and Kinetic Description of Cytochrome c Unfolding Induced by the Interaction with Lipid Vesicles. *Biochemistry 36*, 13122–13132.
47. Addison, A. W., and Stephanos, J. J. (1986) Nitrosyl (III) hemoglobin: autorerduction and spectroscopy. *Biochemistry 25*, 4104–4113.

BI800729W